NASA Technical Memorandum 87659

Supersonic Axial-Force Characteristics of a Rectangular-Box Cavity With Various Length-to-Depth Ratios in a Flat Plate

A. B. Blair, Jr., and Robert L. Stallings, Jr.

APRIL 1986

NASA

NASA Technical Memorandum 87659

Supersonic Axial-Force Characteristics of a Rectangular-Box Cavity With Various Length-to-Depth Ratios in a Flat Plate

A. B. Blair, Jr., and Robert L. Stallings, Jr.
Langley Research Center
Hampton, Virginia

National Aeronautics
and Space Administration

**Scientific and Technical
Information Branch**

1986

INTRODUCTION

Designers of aircraft, missiles, and reentry vehicles encounter numerous problems which require knowledge of the flow characteristics in and around cavities (refs. 1 to 4). A number of studies have been conducted to investigate cavity flow phenomena (refs. 5 to 8). In these studies, flow visualization (schlieren and oil-flow photographs) and surface pressure measurements for various cavity configurations are used to show that two fundamentally different types of flow fields can occur over cavities and that the two types of flow fields are strongly dependent upon cavity length-to-depth ratio l/h.

Pressure coefficient distributions from reference 8 and flow-field sketches for a shallow and deep cavity that are representative of the two types of cavity flow fields are presented in figure 1. For the case of the shallow cavity ($l/h = 19.0$), the pressure distributions are indications of a flow field that is often referred to as a closed, or attached, cavity flow field. For this type of flow field, the flow expands (in a Prandtl-Meyer expansion) around the cavity front face, impinges on the cavity ceiling, and exits ahead of the rear face. The local flow turns through large angles which result in the large pressure gradients shown by the circular symbols in figure 1. Also, low pressures occur on the cavity front face as a result of the flow expansion in the region, and large pressures occur on the rear face, which appears as a forward-facing step to the approaching cavity flow. This combination of pressures on the front and rear faces contributes to large cavity drag coefficients. The pressure distributions shown for the deep cavity ($l/h = 4.0$) are characteristic of a flow field that is often referred to as an open, or detached, cavity flow field. For this cavity, the flow simply bridges the cavity and impinges on the outer edge of the rear face, resulting in relatively small turning angles for the local flow and, consequently, a much more uniform pressure distribution over the cavity ceiling. Also, compared with the closed cavity flow field, larger pressures are measured on the cavity front face and lower pressures are measured on the rear face, both of which contribute to lower cavity drag coefficients for the deep cavity with an open cavity flow field.

The objective of the present investigation was to determine empty-cavity axial-force coefficients associated with deep- and shallow-cavity configurations as part of a continuing effort to study cavity flow-field effects with respect to cavity geometry changes. Axial-force coefficient data were obtained for an empty, rectangular-box cavity with various cavity length-to-depth ratios. The metric-box cavity (i.e., box cavity attached to strain-gage balance) was mounted in a generic flat-plate wing. Variations in cavity length-to-depth ratio were investigated to establish and to verify flow conditions in the cavity for deep- and shallow-cavity configurations. The cavity flow fields generated were of the open (detached) type or closed (attached) type, or both. Large changes in the cavity axial-force coefficient (based on a reference area equal to the cavity rear-face area) reflected these cavity flow-field conditions. In addition, vapor screen photographs that illustrate the complex, three-dimensional nature of the box cavity flow fields were taken during the investigation.

The tests were conducted in the Langley Unitary Plan Wind Tunnel at Mach numbers of 1.50, 2.16, and 2.86. The nominal angle-of-attack range of the flat-plate wing

was -4° to 2° at a Reynolds number of 2.0×10^6 per foot. Measurements included axial-force loads on the metric-box cavity at discrete cavity length-to-depth ratios.

SYMBOLS

The aerodynamic coefficient data are referred to the body-axis system. Values are given in U.S. Customary Units. The measurements and calculations were also made in U.S. Customary Units.

C_A axial-force coefficient, Measured axial force/$q_\infty S$

C_p pressure coefficient, $(p - p_\infty)/q_\infty$

h cavity depth, in.

l cavity length, in.

M free-stream Mach number

p local measured static pressure, lbf/ft^2

p_∞ free-stream static pressure, lbf/ft^2

q_∞ free-stream dynamic pressure, lbf/ft^2

S reference area (based on cross-sectional area of the inside rear-face area of the metric-box cavity), ft^2

x longitudinal station measured from front face of cavity, in. (see fig. 5)

x_1, x_2, x_3 surface lengths for cavity front face, ceiling, and rear face, respectively (see fig. 1)

α angle of attack relative to upper flat-plate wing surface, deg

APPARATUS AND TESTS

Wind Tunnel

Tests were conducted in the low Mach number test section of the Langley Unitary Plan Wind Tunnel, which is a variable-pressure, continuous-flow facility. The test section is approximately 7 ft long and 4 ft square. The nozzle leading to the test section is an asymmetric sliding-block type, which permits a continuous variation in Mach number from about 1.5 to 2.9 (ref. 9).

MODEL DESCRIPTION

Dimensional details of the flat-plate wing and metric-box-cavity model are shown in figure 2. A model photograph is presented as figure 3. To provide a generic parent-body carriage platform, a horizontal steel flat-plate wing was mounted to the tunnel angle-of-attack model support system. A rectangular-box cavity was located in the plate on the longitudinal centerline 10.25 in. downstream from the leading edge.

The plate leading edges had a radius of 0.01 in. and the leading-edge wedge angle was sufficiently small (5°) to ensure shock attachment at $\alpha = 0°$ through the test Mach number range. Also, the flat-plate wing tips were located such that the Mach lines emanating from the tips would clear the cavity for the test Mach number range at $\alpha = 0°$. The boundary layer on the plate surface was artificially tripped with sand grit to ensure fully developed turbulent flow approaching the cavity.

The flat-plate wing cavity was constructed to incorporate an isolated metric rectangular box. As shown in figure 2(a), this metric box was mounted on a balance adapter which was attached to a strain-gage balance. The balance measured total box axial-force loads only. Clearance was maintained between the metric-box and the flat-plate wing cavity walls to avoid fouling. An electrical system was used to indicate fouling. Axial-force loads were obtained on box cavity configurations with various cavity length-to-depth ratios (presented in table I). The various configurations were made by using block inserts and spacers in the metric box. No attempt was made to vary the width of the metric-box cavity.

Test Conditions

Tests were performed at the following tunnel conditions:

Mach number	Stagnation temperature, °F	Stagnation pressure (absolute), lbf/ft^2	Reynolds number, per foot
1.50	125	1051	2.0×10^6
2.16	125	1349	2.0×10^6
2.86	125	1934	2.0×10^6

The dewpoint temperature measured at stagnation pressure was maintained below -30°F to assure negligible condensation effects. All tests were performed with boundary-layer transition strips located 0.40 in. aft of the leading edges. These strip locations were measured in a streamwise direction on the upper surface of the flat-plate wing. The transition strips were approximately 0.062 in. wide and were composed of No. 50 sand grains sprinkled in acrylic plastic (ref. 10).

Measurements

Axial-force loads on the metric-box cavity were measured with an electrical strain-gage balance housed within the flat-plate wing support system and attached to the metric-box-cavity balance adapter (fig. 2(a)). This metric-box cavity with various cavity length-to-depth ratios had the advantage of providing more accurate axial-force measurements than a total metric model since the balance could be sized to accommodate the anticipated forces on the cavity rather than on the complete parent-body configuration. The balance was attached to a sting which, in turn, was rigidly fastened to the flat-plate wing support system. In addition, flat-plate wing cavity pressures were measured with electrical transducers connected to static-pressure orifices located on the front and rear faces of the flat-plate wing cavity.

Accuracy

The accuracy of the individual measured axial-force component based on calibrations and repeatability of data for these tests is estimated to be within the following limits:

M	q_∞, lbf/ft^2	S, ft^2	h, in.	C_A
1.50	451	0.008681	0.500	±0.019156
2.16	439	.008681	.500	±.019680
2.86	373	.008681	.500	±.023162
1.50	451	0.017361	1.000	±0.009579
2.16	439	.017361	1.00	±.009841
2.86	373	.017361	1.00	±.011582

Corrections

The angles of attack were adjusted for tunnel flow misalignment. The axial-force coefficient data were corrected for any pressure differentials in the balance chamber between the front and rear outside faces of the metric-box cavity. No attempt was made to correct for skin-friction axial-force coefficient on the block inserts and spacers in the metric-box cavity; however, the maximum estimated value was within the accuracy levels quoted in the previous section.

RESULTS AND DISCUSSION

Cavity axial-force coefficients as a function of cavity l/h are presented in figure 4. These results are presented for $\alpha = 0°$ and for the three test Mach numbers. In order to expand the cavity geometry length and depth envelope of the present tests, data are also included from the integrated pressure data of reference 8. Since the major contributors to cavity axial force are the pressure forces acting on the cavity front and rear faces, the coefficients shown in figure 4 for all data are based on reference areas equal to the rear- (or front-) face area. The results for $M = 1.50$ (fig. 4(a)) show that for $l/h \leq 10$ relatively low values of C_A are measured, indicative of open cavity flow. For $10 < l/h < 12$, the cavity flow field transitions from open flow to closed flow, a change which results in an abrupt increase in C_A consistent with the trend discussed previously based on the pressure distributions shown in figure 1. The C_A increases by a factor of approximately 4. Similar trends are shown in figure 4(b) for $M = 2.16$, except that the transition from an open to a closed cavity flow field occurs at $12 < l/h < 14$ and C_A increases by a factor of approximately 6. The data shown at this Mach number cover the widest range of cavity lengths and cavity depths and the good correlation of all the data suggests (1) that the correct reference area (the rear-face area) was selected to compare the data and (2) that l/h is the dominant factor affecting the switching of the flow field from one type to the other. The results presented for $M = 2.86$ (fig. 4(c)) show that the transition value of l/h still occurs between 12 and 14 and that the ΔC_A associated with the flow field switching from open to closed is approximately the same as that measured at $M = 2.16$.

Cavity vapor-screen photographs for $M = 2.16$ and $\alpha = 0°$ that were taken by use of the techniques described in reference 11 are presented in figure 5. The light screens illuminating the flow were in a plane perpendicular to the flat-plate surface and the cavity longitudinal centerline. The photographs were taken with a camera located downstream from and positioned above the model looking upstream. Photographs are shown for a deep cavity ($l/h = 6.40$) that had an open cavity flow field and for a shallow cavity ($l/h = 24.00$) that had a closed cavity flow field. Both cavities had a length of 12.00 in. and the depth was varied to obtain the indicated values of l/h. The photographs presented are for the same longitudinal locations downstream of both cavity leading edges.

The vapor-screen photographs for the shallow cavity having a closed flow field illustrate the complexity and three-dimensionality of this type flow field, including the formation of a pair of well-defined vortices at the edges of the cavity and the existence of several shock wave formations resulting from the large turning angles of the local flow. Three-dimensional computational procedures would be required to describe theoretically the closed cavity flow field. The photographs shown for the deep cavity with an open flow field indicate a less complex flow field, as there are no apparent shock waves and vortices.

The variation of cavity C_A with angle of attack for various constant values of l/h at two cavity depths is presented in figure 6. The data shown in figure 6(a) ($h = 0.500$ in.) are for a sufficiently wide range of cavity l/h that the values of C_A are representative of both open- and closed-type cavity flow fields. With the exception of $l/h = 12.00$ at $M = 1.50$ and 2.86, the data indicate that the cavity flow fields remain of the same type through the angle-of-attack range. At $M = 1.50$, a switch from an open to a closed flow field occurs with increasing angle of attack for the $l/h = 12.00$ cavity, whereas at $M = 2.86$ a switch from a closed to an open flow field occurs with increasing angle of attack. This apparently anomalous behavior of the flow field probably occurs because $l/h = 12.00$ is very close to a critical value at which flow-field switching occurs, and for this value of l/h the flow field can be of either type (i.e., a bistable cavity flow field), with only small perturbations required to cause a switch from one type to the other. The results presented in figure 6(b) for the cavities with $h = 1.000$ in. indicate that only open cavity flow occurs for the test range of l/h and angles of attack.

It should be noted that as angle of attack is changed from 0°, the local Mach number and dynamic pressures on the flat-plate wing surface change and also the plate flow field deviates from a two-dimensional type of flow field. These changes in the local flow conditions are reflected in the change with angle of attack of the cavity axial-force coefficients shown in figure 6 for the cases in which the type of cavity flow field remains unchanged.

CONCLUSIONS

A wind-tunnel investigation has been conducted at Mach numbers of 1.50, 2.16, and 2.86 to obtain axial-force coefficient data on a metric rectangular-box cavity with various length-to-depth ratios. The model was tested at angles of attack from -4° to 2°. The results were summarized to show variations in cavity axial-force coefficient for deep- and shallow-cavity configurations with detached and attached cavity flow fields, respectively. The results of the investigation were as follows:

1. For a wide range of cavity lengths and depths, good correlations of the cavity axial-force coefficients (based on a reference area equal to the cavity rear-face area) were obtained when these coefficients were plotted as a function of cavity length-to-depth ratio.

2. Abrupt increases in the cavity axial-force coefficients at an angle of attack of 0° reflected the transition of the cavity flow field from an open (detached) flow field to a closed (attached) flow field.

3. Cavity length-to-depth ratio at an angle of attack of 0° was the dominant factor affecting the switching of the cavity flow field from one type to the other.

4. The type of cavity flow field (open or closed) was not dependent on the test angles of attack except near the critical value of length-to-depth ratio.

NASA Langley Research Center
Hampton, VA 23665-5225
January 27, 1986

REFERENCES

1. Nestler, D. E.: An Experimental Study of Cavity Flow on Sharp and Blunt Cones at Mach 8. AIAA-81-0335, Jan. 1981.

2. Nestler, Donald E.: An Experimental Study of Hypersonic Cavity Flow. J. Spacecr. & Rockets, vol. 19, no. 3, May-June 1982, pp. 195-196.

3. Catani, Umberto; Bertin, John J.; De Amicis, Roberto; Masullo, Sergio; and Bouslog, Stanley A.: Aerodynamic Characteristics for a Slender Missile With Wrap-Around Fins. J. Spacecr. & Rockets, vol. 20, no. 2, Mar.-Apr. 1983, pp. 122-128.

4. Kaufman, Louis G., II; Maciulaitis, Algirdas; and Clark, Rodney L.: Mach 0.6 to 3.0 Flows Over Rectangular Cavities. AFWAL-TR-82-3112, U.S. Air Force, May 1983. (Available from DTIC as AD A134 579.)

5. Charwat, A. F.; Roos, J. N.; Dewey, F. C., Jr.; and Hitz, J. A.: An Investigation of Separated Flows - Part I: The Pressure Field. J. Aeronaut. Sci., vol. 28, no. 6, June 1961, pp. 457-470.

6. Charwat, A. F.; Roos, J. N.; Dewey, F. C., Jr.; and Hitz, J. A.: An Investigation of Separated Flows - Part II: Flow in the Cavity and Heat Transfer. J. Aeronaut. Sci., vol. 28, no. 7, July 1961, pp. 513-527.

7. McDearmon, Russell W.: Investigation of the Flow in a Rectangular Cavity in a Flat Plate at a Mach Number of 3.55. NASA TN D-523, 1960.

8. Stallings, Robert L., Jr.: Store Separations From Cavities at Supersonic Flight Speeds. J. Spacecr. & Rockets, vol. 20, no. 2, Mar.-Apr. 1983, pp. 129-132.

9. Jackson, Charlie M., Jr.; Corlett, William A.; and Monta, William J.: Description and Calibration of the Langley Unitary Plan Wind Tunnel. NASA TP-1905, 1981.

10. Stallings, Robert L., Jr.; and Lamb, Milton: Effects of Roughness Size on the Position of Boundary-Layer Transition and on the Aerodynamic Characteristics of a 55° Swept Delta Wing at Supersonic Speeds. NASA TP-1027, 1977.

11. Morris, Odell A.; Corlett, William A.; Wassum, Donald L.; and Babb, C. Donald: Vapor-Screen Technique for Flow Visualization in the Langley Unitary Plan Wind Tunnel. NASA TM-86384, 1985.

TABLE I. CAVITY VARIABLES OF PRESENT TEST

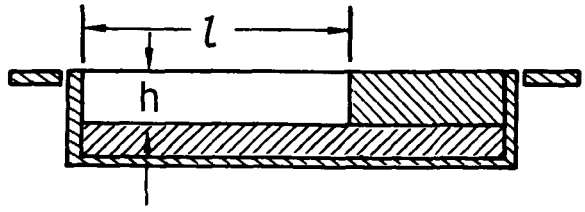

h, in.	l, in.	l/h	h, in.	l, in.	l/h
0.500	2.00	4.00	1.000	2.00	2.00
↓	3.00	6.00	↓	4.00	4.00
	4.00	8.00		6.00	6.00
	5.00	10.00		7.07	7.07
	6.00	12.00		8.00	8.00
	7.00	14.00		10.00	10.00
	7.07	14.14	1.875	7.07	3.77
	9.00	18.00	1.875	12.00	6.40
↓	12.00	24.00			

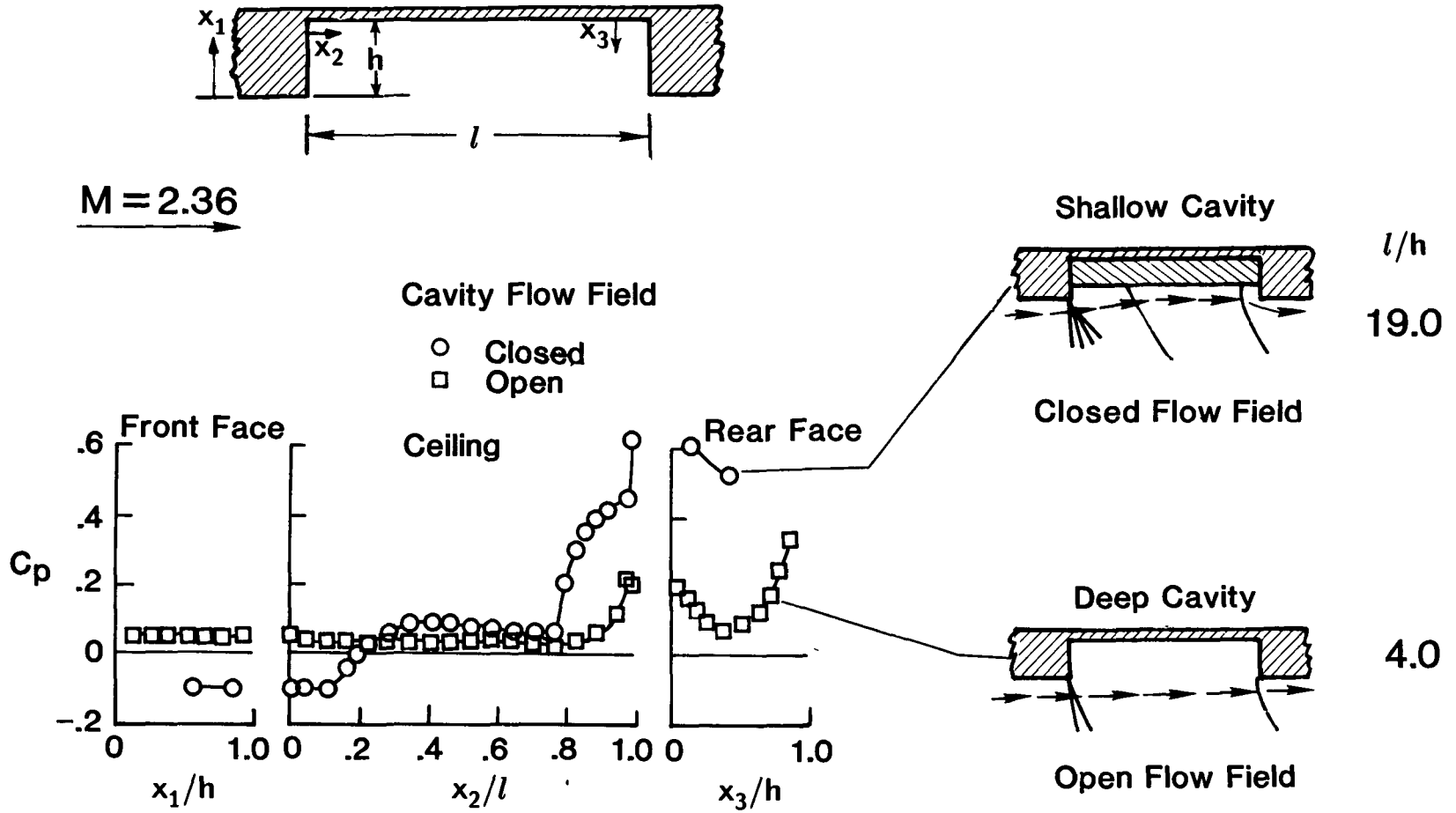

Figure 1.- Pressure coefficient distributions for shallow and deep cavities with closed and open flow fields (from ref. 8).

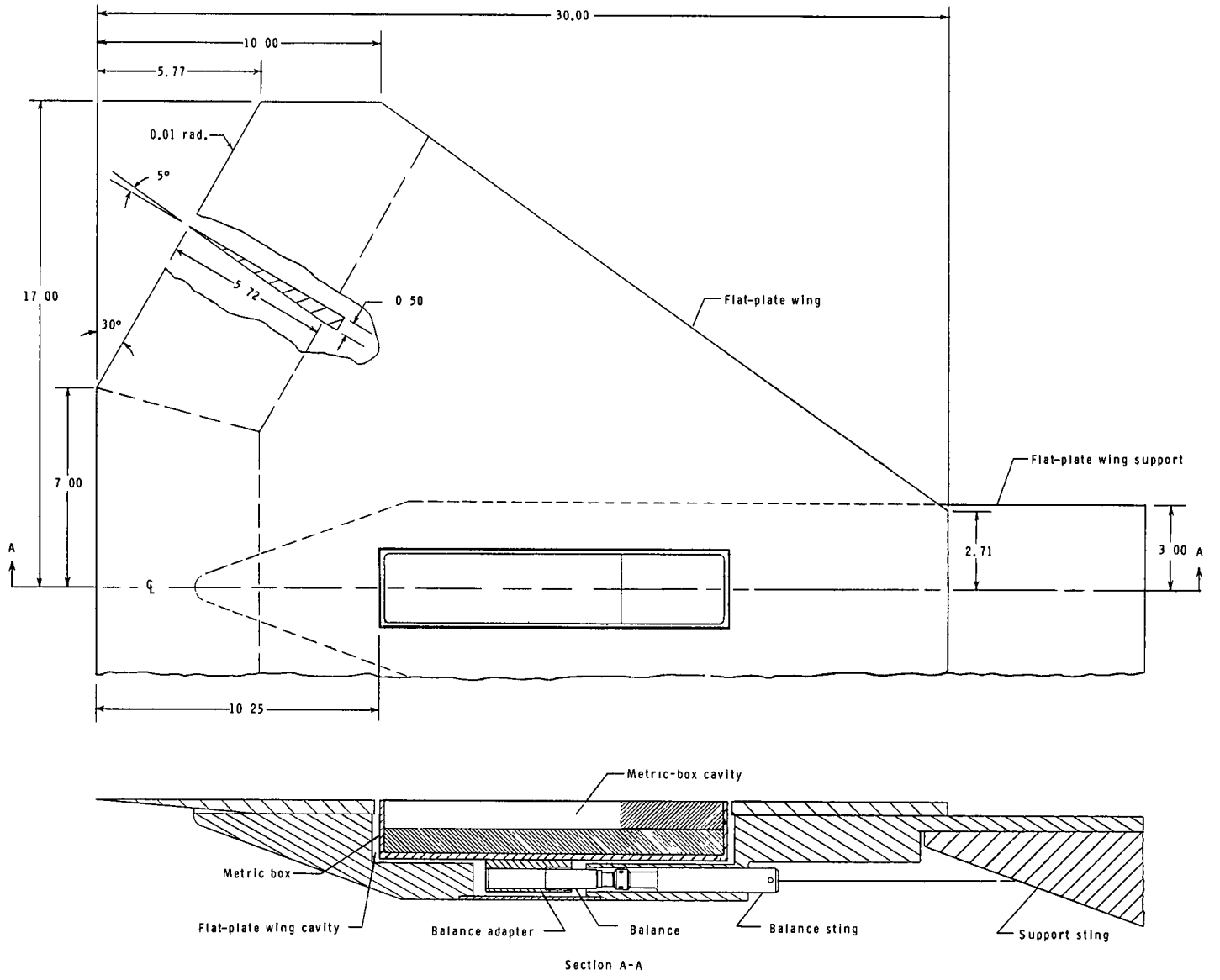

(a) Flat-plate wing with metric box.

Figure 2.- Model details. All dimensions are given in inches unless otherwise indicated.

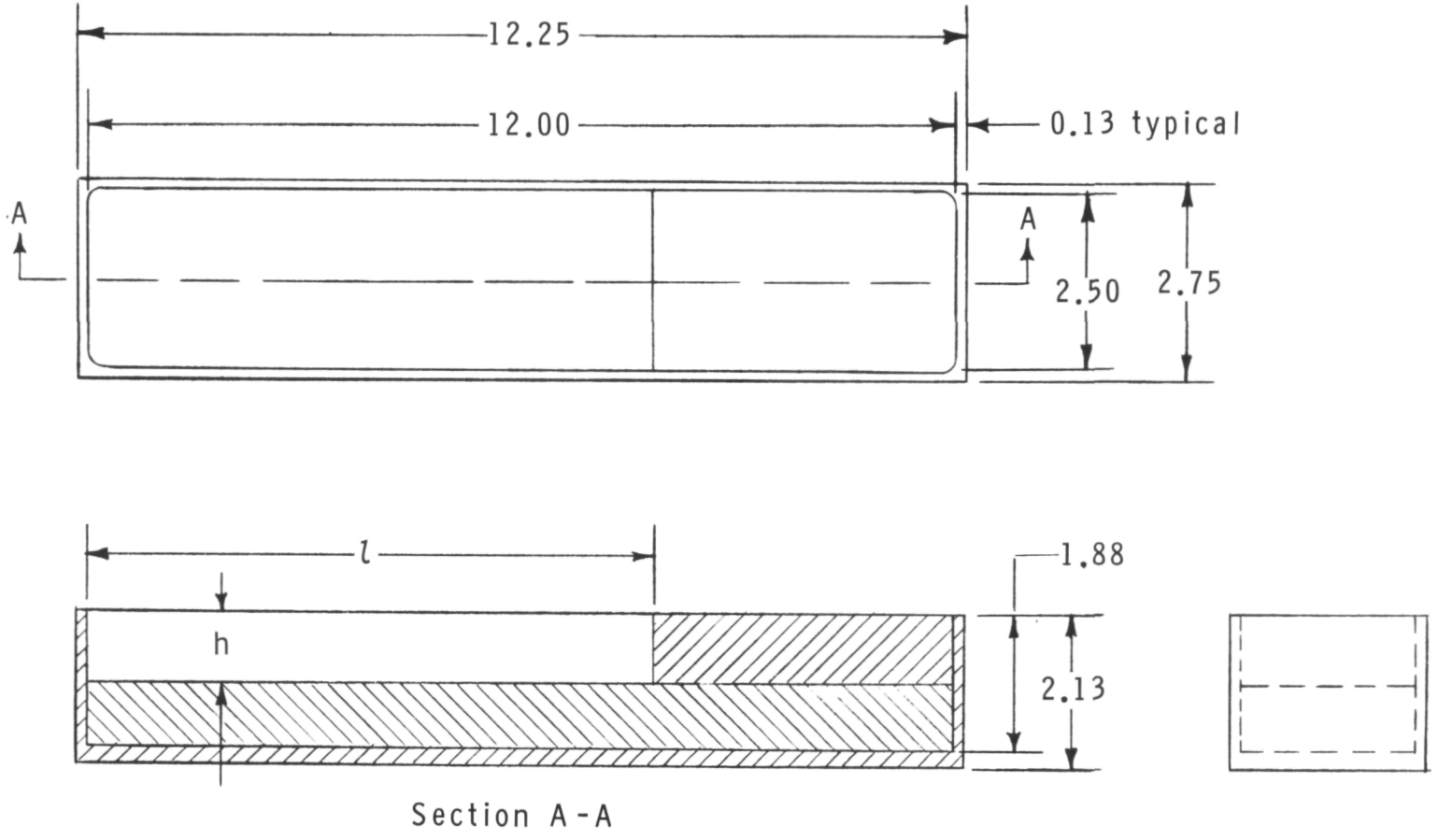

(b) Metric-box cavity.

Figure 2.- Concluded.

L-83-2,771

Figure 3.- Model photograph.

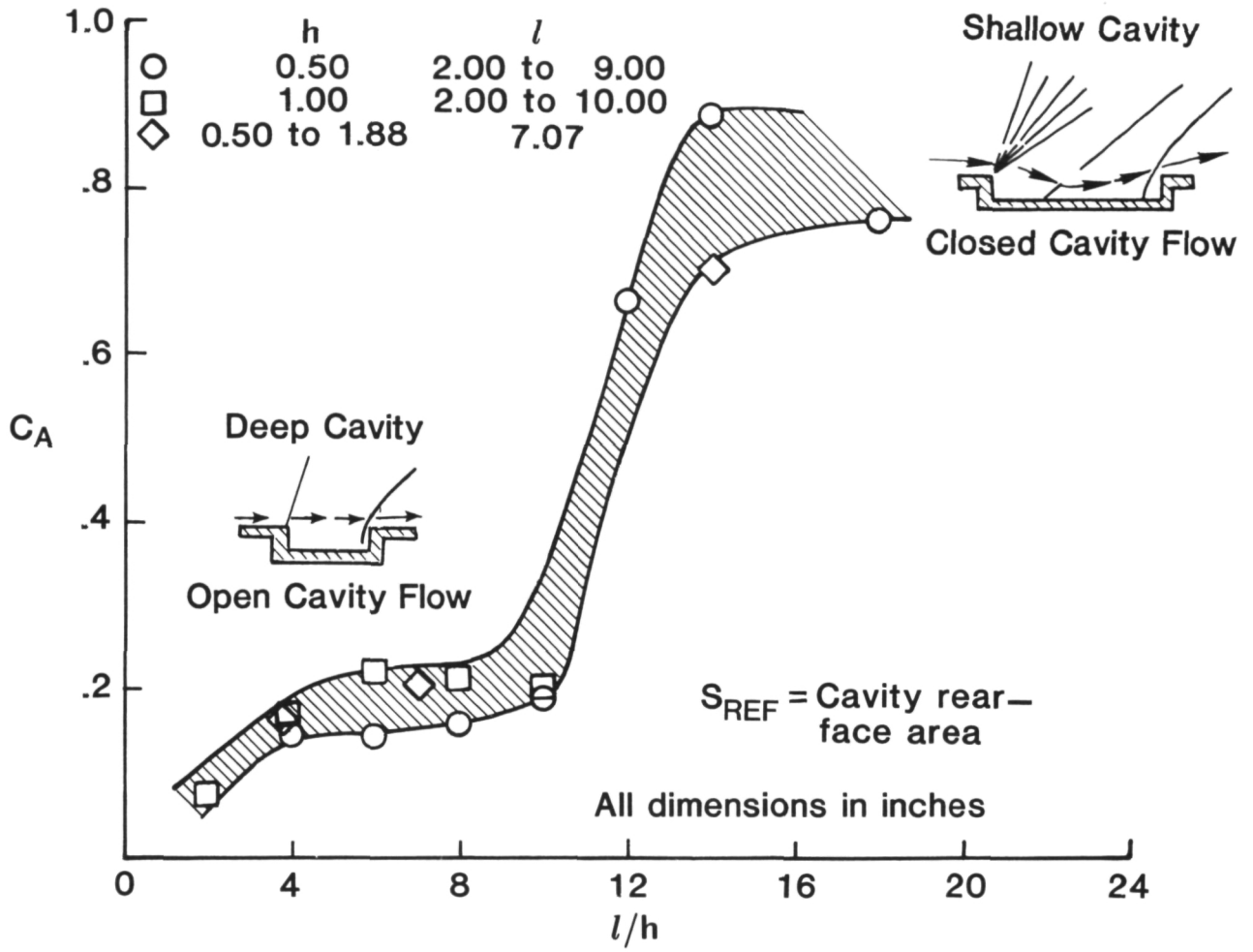

(a) M = 1.50.

Figure 4.- Summary of C_A values as function of cavity l/h. $\alpha = 0°$.

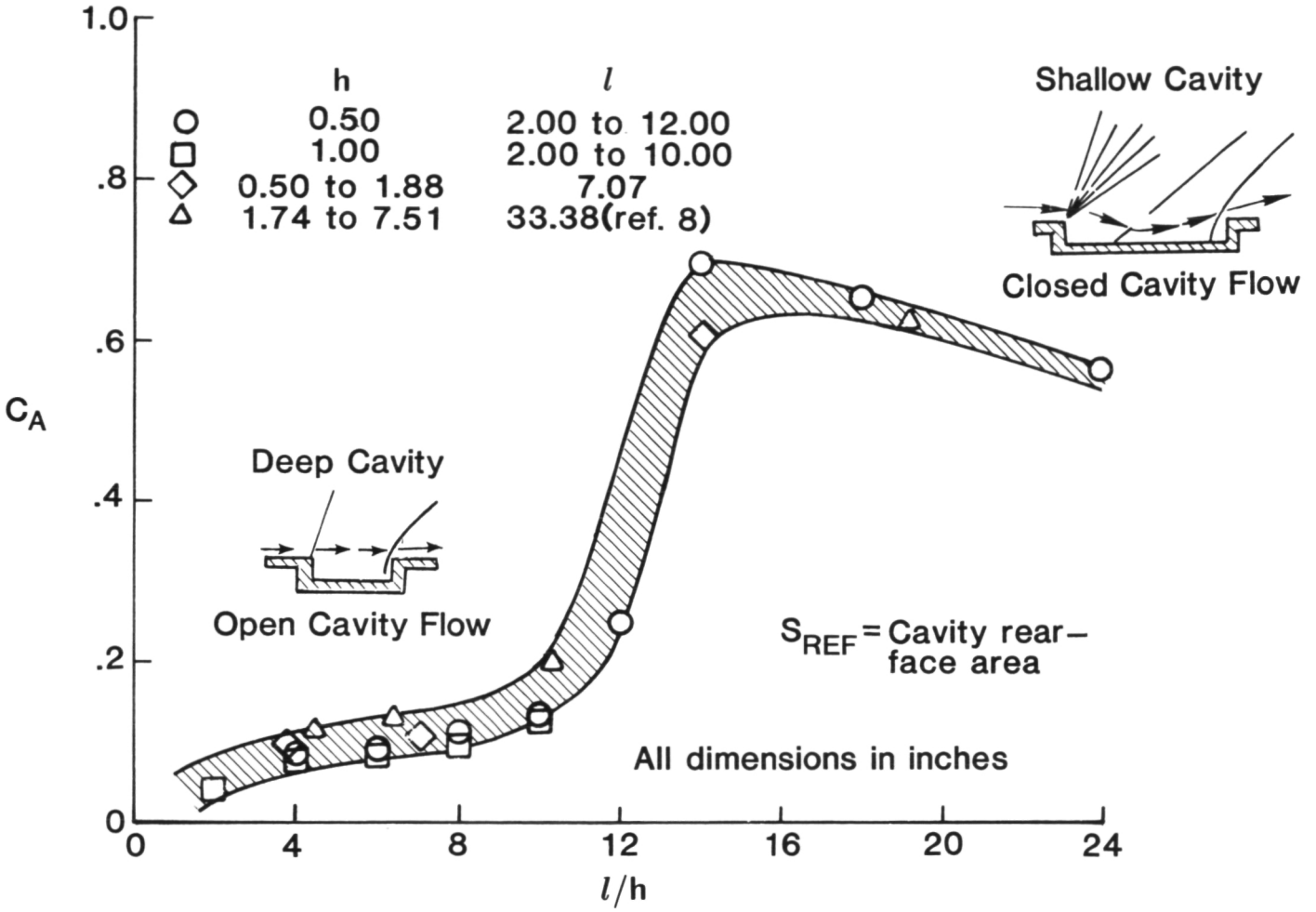

(b) M = 2.16.

Figure 4.- Continued.

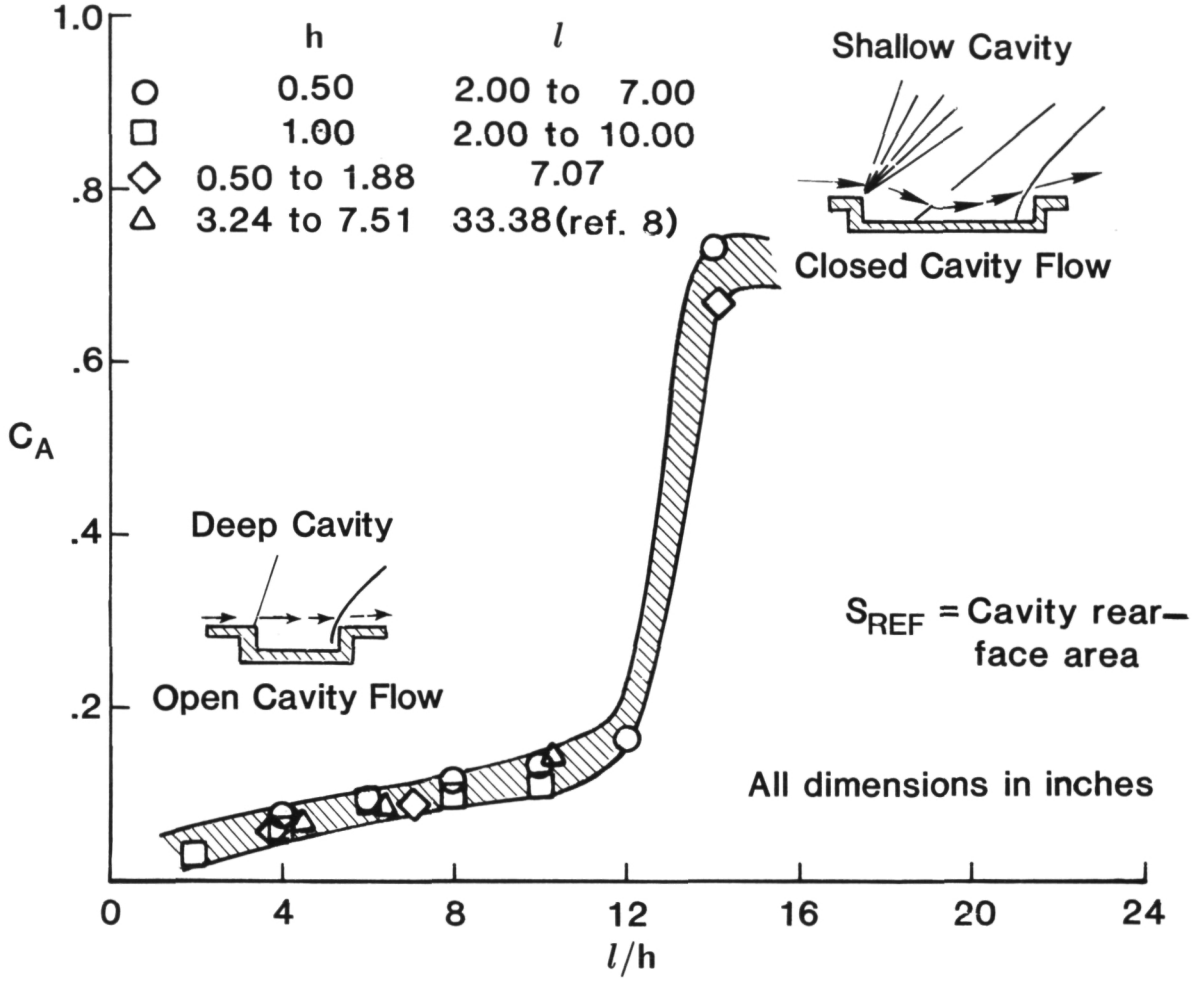

(c) M = 2.86.

Figure 4.- Concluded.

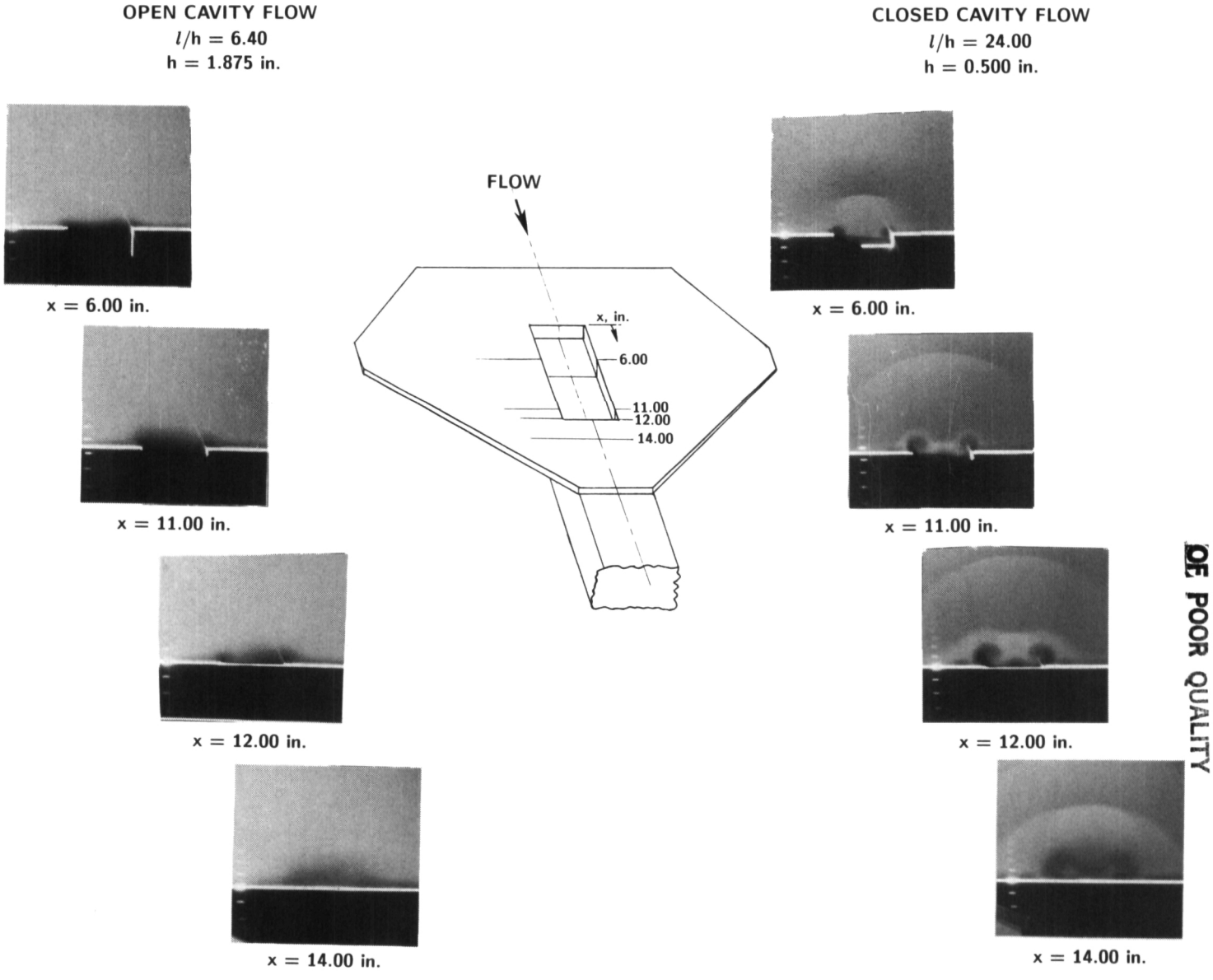

L-86-305

Figure 5.- Cavity vapor-screen photographs. M = 2.16; $\alpha = 0°$.

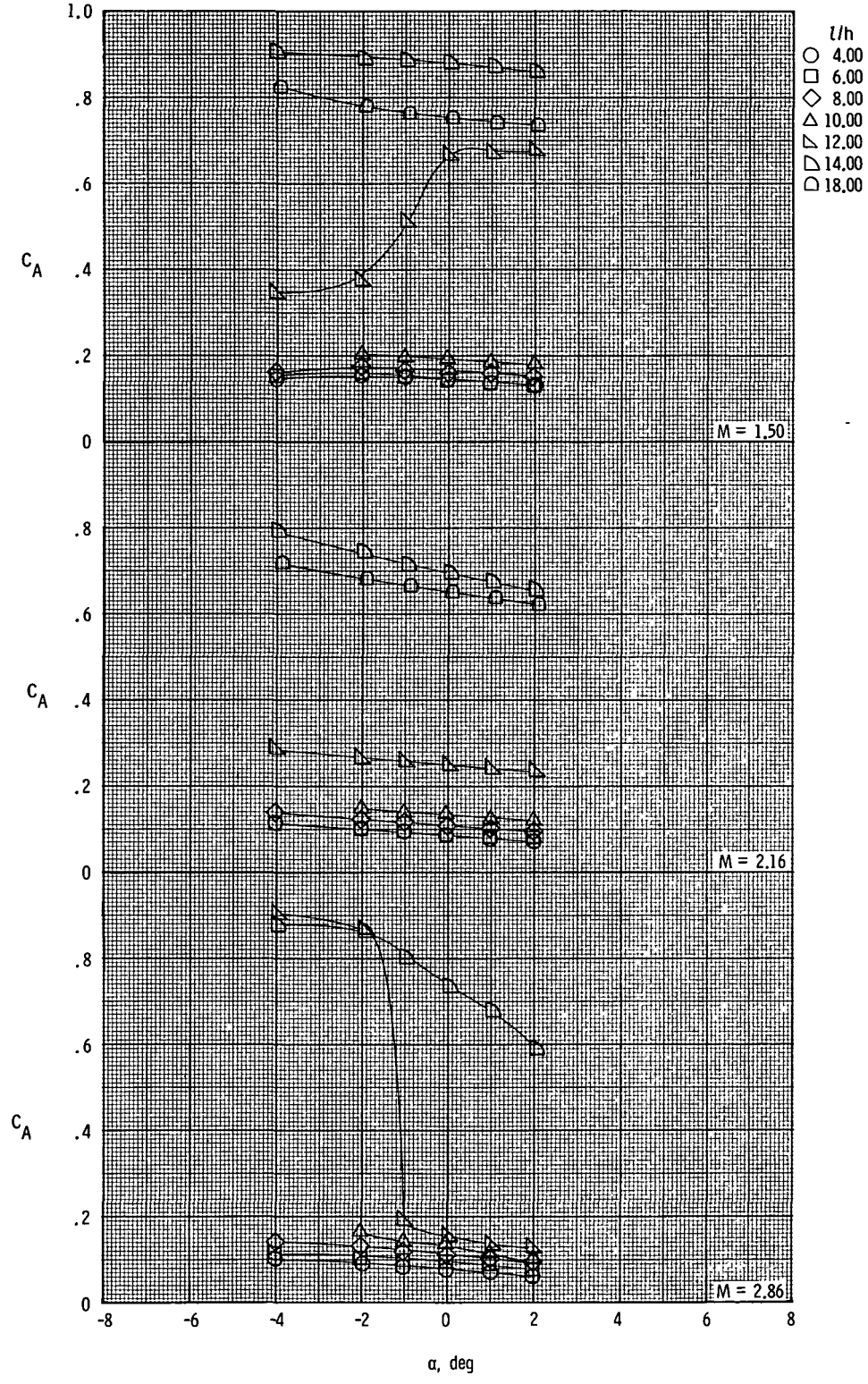

(a) h = 0.50 in.

Figure 6.- Effects of cavity l/h on axial-force coefficients with angle of attack.

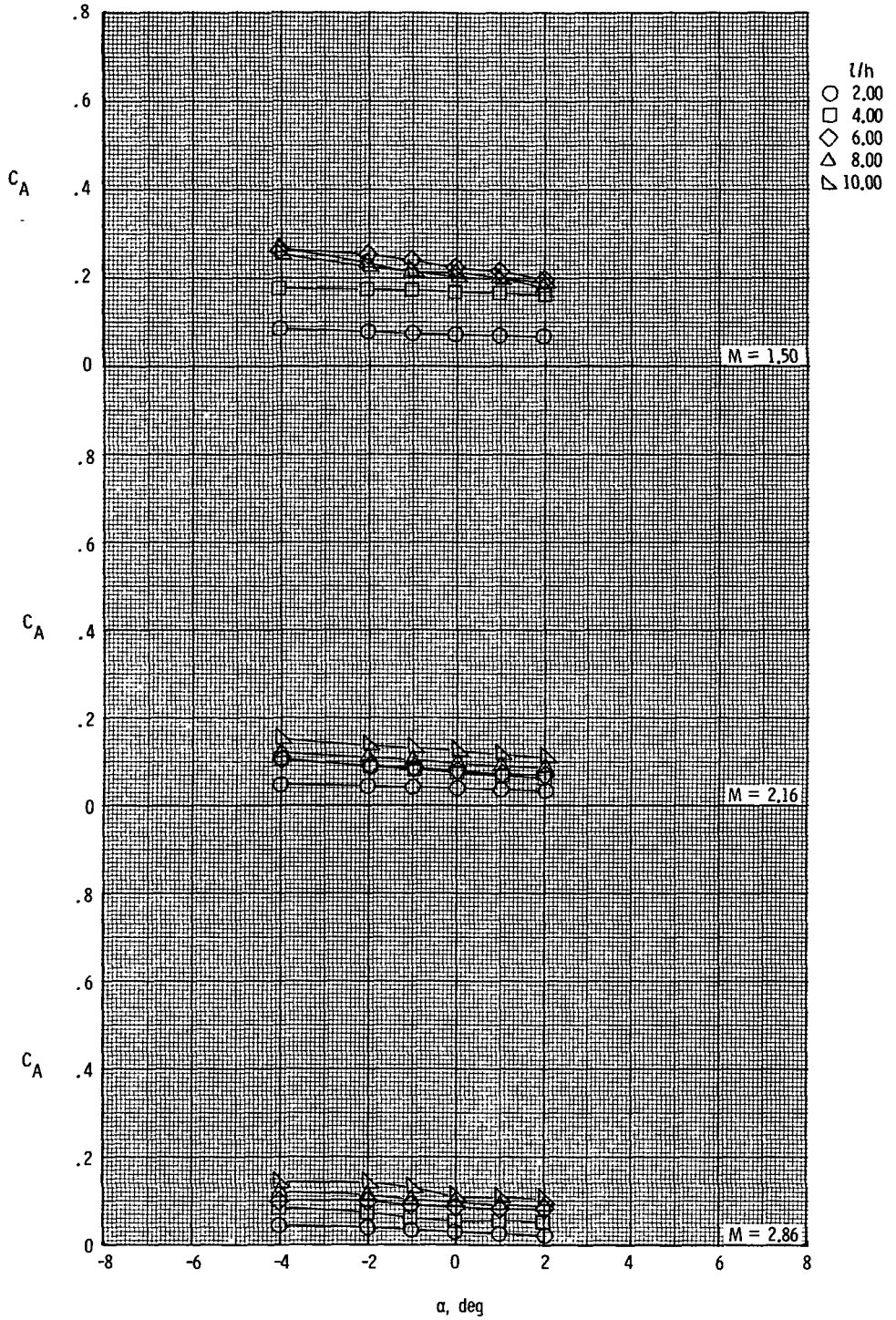

(b) h = 1.00 in.

Figure 6.- Concluded.

1. Report No.	2. Government Accession No.	3. Recipient's Catalog No.
NASA TM-87659		

4. Title and Subtitle	5. Report Date
Supersonic Axial-Force Characteristics of a Rectangular-Box Cavity With Various Length-to-Depth Ratios in a Flat Plate	April 1986
	6. Performing Organization Code: 505-43-23-02
7. Author(s): A. B. Blair, Jr., and Robert L. Stallings, Jr.	8. Performing Organization Report No.: L-16075
	10. Work Unit No.
9. Performing Organization Name and Address: NASA Langley Research Center, Hampton, VA 23665-5225	11. Contract or Grant No.
	13. Type of Report and Period Covered: Technical Memorandum
12. Sponsoring Agency Name and Address: National Aeronautics and Space Administration, Washington, DC 20546-0001	14. Sponsoring Agency Code

15. Supplementary Notes

16. Abstract

A wind-tunnel investigation has been conducted at Mach numbers of 1.50, 2.16, and 2.86 to obtain axial-force data on a metric rectangular-box cavity with various length-to-depth ratios. The model was tested at angles of attack from -4° to 2°. The results are summarized to show variations in cavity axial-force coefficient for deep- and shallow-cavity configurations with detached and attached cavity flow fields, respectively. The results of the investigation indicate that for a wide range of cavity lengths and depths, good correlations of the cavity axial-force coefficients (based on cavity rear-face area) are obtained when these coefficients are plotted as a function of cavity length-to-depth ratio. Abrupt increases in the cavity axial-force coefficients at an angle of attack of 0° reflect the transition from an open (detached) cavity flow field to a closed (attached) cavity flow field. Cavity length-to-depth ratio is the dominant factor affecting the switching of the cavity flow field from one type to the other. The type of cavity flow field (open or closed) is not dependent on the test angles of attack except near the critical value of length-to-depth ratio.

17. Key Words (Suggested by Author(s))	18. Distribution Statement
Supersonic aerodynamics Supersonic cavity flow Open cavity flow Closed cavity flow Box-shaped cavities Cavity drag	Unclassified - Unlimited Subject Category 02

19. Security Classif. (of this report)	20. Security Classif. (of this page)	21. No. of Pages	22. Price
Unclassified	Unclassified	19	A02

For sale by the National Technical Information Service, Springfield, Virginia 22161

NASA-Langley, 1986